The low temperature and high density ignition in the helical reactor FFHR2m based on LHD experiments

O. Mitarai[(1)], A. Sagara[(2)], N. Ashikawa[(2)], R. Sakamoto[(2)], M. Yoshinuma[(2)], M. Goto[(2)], T. Morisaki[(2)], T. Masuzaki[(2)], K. Ida[(2)], S. Morita[(2)], M. Osakabe[(2)], K. Tanaka[(2)], K. Nagaoka[(2)], N. Ohyabu[(2)], A. Komori[(2)], and O. Motojima[(2)]

(1) Liberal Arts Education Center, Kumamoto Campus, Tokai University, 9-1-1 Toroku, Kumamoto 862-8652, Japan
(2) National Institute for Fusion Science, 322-6 Oroshi-cho, Toki, 509-5292, Japan

E-mail contact of main author: omitarai@ktmail.tokai-u.jp

Abstract New control method of the unstable operating point in the helical reactor FFHR makes the ignition study on the high density and low temperature operation possible. It is a proportional-integration-derivative (PID) control of the fueling with the error of the fusion power of $e(P_f)= -(P_{fo}-P_f)$, which can stabilize the unstable operating point. Here $P_{fo}(t)$ is the fusion power set value and $P_f(t)$ is the measured fusion power. Although the large parameter variation would lose its control due to the inherently unstable nature, it is still possible to control the ignited operation with pellet injection if the pellet size is smaller than 16 mm. As sensitivity analysis on other parameters makes the helium ash confinement time ratio crucial, preliminary experimental results on helium ash measurement in LHD are also presented. We finally discovered that major plasma parameters for 1.9 GW fusion power are close to plasma parameters independently achieved in LHD experiments.

1. Introduction

Remarkable result of the super dense core (SDC) plasma up to $1.1\text{x}10^{21}$ m^{-3} has been obtained in recent large helical device (LHD) pellet injection experiments [1][2]. In Wenderstein 7-AX, the high density H-mode with $4\text{x}10^{20}$ m^{-3} has also been produced [3]. Such low temperature and high density operation is generally advantageous to reduce the divertor heat flux in both tokamak and helical reactors. However, an operation in the low temperature and high-density ignition regime usually suffers from the thermal instability, where the operating point moves to the higher or lower temperature side. New control algorithm using the simple PID control on fueling has been proposed to overcome the thermal instability in the LHD type helical reactor (FFHR2m) [4]. Owing to the simple and comprehensive algorithm which does not need any linearization of the particle and power balance equations, this control method can be implemented in a reactor where fusion power measurement provides the feedback signals for PID control of fueling.

Many stabilizing methods of the thermally unstable ignition have been proposed so far, using such as fueling [5], impurity injection [6] and heating power modulations [7], and these combinations. In these controls, 0-dimensional equations of the particle and power balance equations have been linearized around the unstable operating point, and then stabilizing techniques such as H-infinity control [8], non-linear control method [9], and neural network control [10] have been applied. In these methods, linearization is necessary in many equations and hence it may be difficult to apply it to the actual situation. In the previous studies, only stabilization around the unstable operating point has been shown, but the access to the unstable operating point from the zero temperature and zero density has not been demonstrated.

In this work we have found that although the large parameter variation would lose its control due to the inherently unstable nature, control can be done for various disturbances to some extents. We have also demonstrated that a fueling at the discrete time for simulating the pellet injection can control the ignition access and steady state operation at the thermally unstable regime despite its oscillatory nature using PID pellet fueling control. We finally discovered that major plasma parameters for FFHR2m with 1.9 GW fusion power output are

close to plasma parameters independently achieved in LHD experiments [1].

2. Zero-dimensional equations and density profiles of SDC plasma

In this analysis, the global power balance equation is used,

$$\frac{dW}{dt} = P_{EXT} - \left(P_L + P_B + P_S - P_\alpha\right) \quad (1)$$

where P_{EXT} is the external heating power, P_L is the total plasma conduction loss, P_B is the total bremsstrahlung loss, P_S is the total synchrotron radiation loss, which is negligible in the low temperature operation, and P_α is the total alpha heating power. The ISS95 confinement scaling is used for the plasma conduction loss where γ_{ISS} represent the confinement enhancement factors over the ISS95 scaling. POPCON is the contour map of the heating power of $P_{HT} = \left(P_L + P_B + P_S - P_\alpha\right)$ plotted on the n-T plane. Sudo density limit scaling on the line density of the core plasma with the density limit factor of γ_{SUDO}=5.5 is used as a measure of density. The external heating power is preprogrammed during the whole discharge, because it is difficult to use the density limit scaling for feedback control of the external heating power. This is different from operations on stable ignition boundary [11]. In the power balance equation the equal ion and electron temperature was assumed due to very high density.

The combined particle balance equation using the charge neutrality condition is

$$\frac{dn_e(0)}{dt} = \frac{1}{1-8f_O}\left[(1+\alpha_n)S_{DT}(t) - \left\{\frac{f_D + f_T}{\tau_p^*} + \frac{2f_\alpha}{\tau_\alpha^*}\right\}n_e(0)\right] \quad (2)$$

where f_o is the impurity fraction, α_n is the density profile factor, S_{DT} is the D-T fueling rate, f_D is the deuterium fraction, f_T is the tritium fraction, f_α is the alpha ash fraction, τ_p* is the D-T fuel particle confinement time, and τ_α* is the He ash confinement time. The helium ash confinement time ratio of τ_α^*/τ_E=3, and the fuel particle confinement tome ratio of τ_p^*/τ_E=3 have been used in the helium ash particle balance equation unless otherwise noted. We assumed the box type density profile for SDC plasma using hyperbolic tangent as shown in Fig. 1, and used the broad temperature profile with α_T=0.25 as observed in LHD experiments [3].

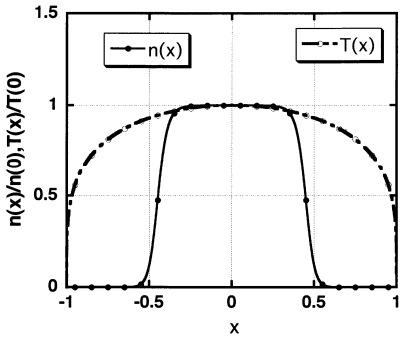

FIG. 1. Assumed SDC density and temperature profiles.

2. Unstable ignition control algorithm and pellet size

Stable ignition in FFHR reactor is controlled by the continuous D-T fueling rate:

$$S_{DT}(t) = S_{DT0}\left\{e_{DT}(P_f) + \frac{1}{T_{int}}\int_0^t e_{DT}(P_f)dt + T_d\frac{de_{DT}(P_f)}{dt}\right\}G_{fo}(t) \quad (3)$$

where the PID control is used based on the fusion power error of $e_{DT}(P_f) = +(1-P_f/P_{fo})$, where $P_{fo}(t)$ is the fusion power set value and $P_f(t)$ is the measured fusion power [11]. However, in the unstable regime, $e_{DT}(P_f)= -(1-P_f/P_{fo})$ can stabilize the thermal instability [4].

This behavior is understood as shown in POPCON in Fig. 2 for the continuous fueling. When P_f is larger than P_{fo}, the operating point (A) moves toward the higher density and lower temperature side. This operating point slightly shifts to the higher temperature side due to ignition nature between (A) and (B). When it enters in the sub-ignition regime (B), it goes

to the lower temperature side due to sub-ignition nature and crosses the constant P_{fo} line (C). The fueling is now decreased and the operating point proceeds to the lower density and higher temperature side, and goes into the ignition regime (D), and crosses the constant P_{fo} line. Thus, oscillations take place and are damped away.

On the other hand, for pellet injection the fueling is digitized. Fueling rate is given by

$$\begin{cases} S_{DT}(t) = S_{DTpellet} & for\ Error(P_f) > 0 \\ S_{DT}(t) = 0 & for\ Error(P_f) \le 0 \end{cases}$$

where $S_{DTpellet}$ is the fueling rate by one pellet as given below, and Error(P_f) is the PID signal based on the fusion power error of $e_{DT}(P_f) = -(1-P_f/P_{fo})$ as

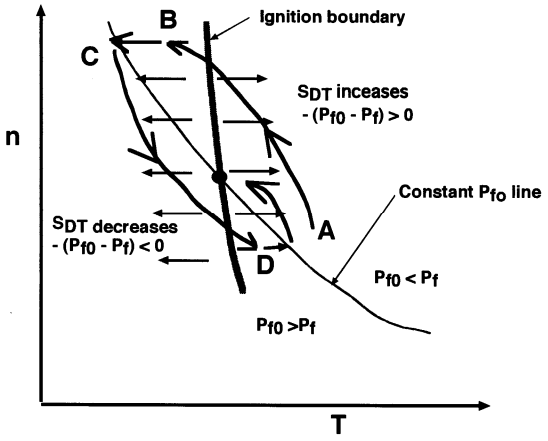

FIG. 2. Schematic movement of the operating point around the unstable ignition point on POPCON.

$$Error(P_f) = \left\{ e_{DT}(P_f) + \frac{1}{T_{\text{int}}} \int_0^t e_{DT}(P_f)dt + T_d \frac{de_{DT}(P_f)}{dt} \right\}$$

As the D-T solid molar volume is 19.88 mm^3/mol [12], D-T ice density is given by $\{6.02x10^{23}x2\}/19.88$ [mm^3/mol]=$6.05x10^{28}$ m^{-3}. For the pellet size of L_p=12 mm diameter and L_p=12 mm length, the total D-T particle number is $N_{pell}=p(L_p/2)^2L_px6.05x10^{28}=82x10^{21}$ m^{-3}. Therefore, fueling rate per volume is $S_{DTpell}=N_{pell}/V_p= 0.99x10^{20}$ m^{-3}/(1 pellet pulse) (see Fig 3-(d)). For the pellet size of 14 mm and 16 mm diameter, $S_{DTpell}= 1.57x10^{20}$ m^{-3}/(1 pellet pulse) (see Fig 7-(d)) and $S_{DTpell}=2.35x10^{20}$ m^{-3}/(1 pellet pulse) (see Fig 5-(d)) are obtained, respectively. Minimum repetition time of pellet injection is 240 ms. Detailed pellet injection algorithm was described in the reference 13.

3. Ignition access to the unstable operating point with pellet injection

Figure 3 shows the temporal evolution of plasma parameters for the pellet size of L_p=12 mm in FFHR2m with R=14 m, $\bar{a}$ =1.73 m, B_o=6 T, P_f=1.9 GW and γ_{ISS}=1.6. For the fusion power rise-up time of $\Delta\tau_{rise}$=20 sec and the maximum external heating power of P_{EXT}=80 MW, the time averaged density is initially built up to ~$0.6x10^{21}$ m^{-3} by the density feedback (NGW trace) until 12.8 s and then raised up to n(0)~$1x10^{21}$ m^{-3} by the fusion power control switched on at 12.8 s. The external heating power is preprogrammed to decrease it to 0 at 24 sec because the feedback control is not used as in the stable operation. We see that even by fueling at the discrete time the ignition access is possible. When the density is increased by one pellet, the temperature is dropped. Their variations are out of phase due to adiabatic process in a short time. We found that the density variation of $\Delta n\sim 2.5x10^{19}$ m^{-3} is allowed for ignited operation. The time averaged peak temperature at the steady state is $T_i(0)$~6.4 keV, the volume averaged beta value is $<\beta>\sim$ 2.5 %, the helium ash fraction is 5.4 %, the effective charge is Z_{eff}~1.52, the average neutron wall loading is Γ_n~1.5 MW/m^2, the ratio of the bremsstrahlung loss power P_B to the alpha heating power P_α is P_B/P_α ~ 71 %, reducing the divertor heat load to Γ_{div}~5.4 MW/m^2 for the 10cm width of the divertor plate. Other parameters are also listed in Table 1. As the confinement time is increased due to high-density operation, the plasma conduction loss P_L is reduced.

In Fig. 4 is shown the operation path to the unstable ignition point on POPCON corresponding to Fig. 3. The operation is stabilized by cooling with fueling and by heating with

the fueling reduction, which is controlled by the error of the fusion power $e_{DT}(P_f) = -(1- P_f/P_{fo})$. We see that the operating point never go beyond 6.3 keV, which may avoid the neo-classical transport.

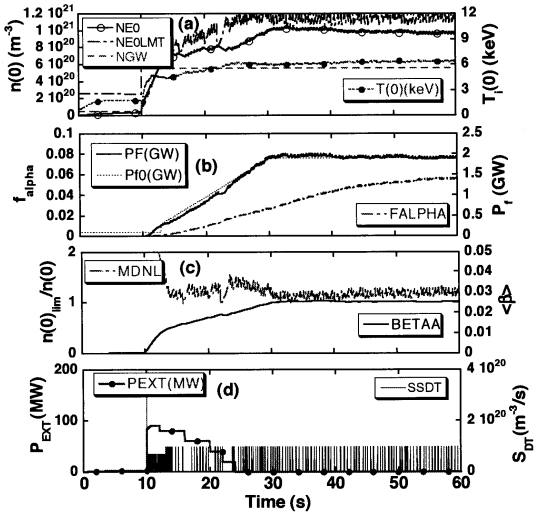

FIG. 3. Temporal evolution of the plasma parameters with pellet injection with pellet size of 12 mm. (a) Peak temperature, peak density, density limit, (b) alpha ash fraction, fusion power and its set value, (c) density limit margin, beta value, and (d) D-T pellet fueling rate, and the heating power. T_d=0.26s and T_{int}=8s.

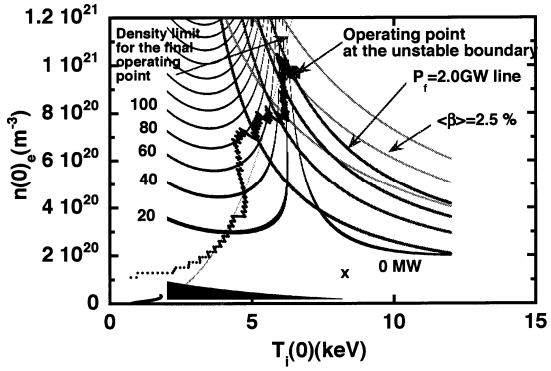

FIG. 4. The operation path to the unstable ignition point on POPCON corresponding to Fig. 3.

For the larger pellet size of 16 mm, temporal evolution and POPCON are shown in Fig. 5 and Fig. 6, respectively. The density variation becomes as large as $\Delta n \sim 8 \times 10^{19}$ m^{-3}, but

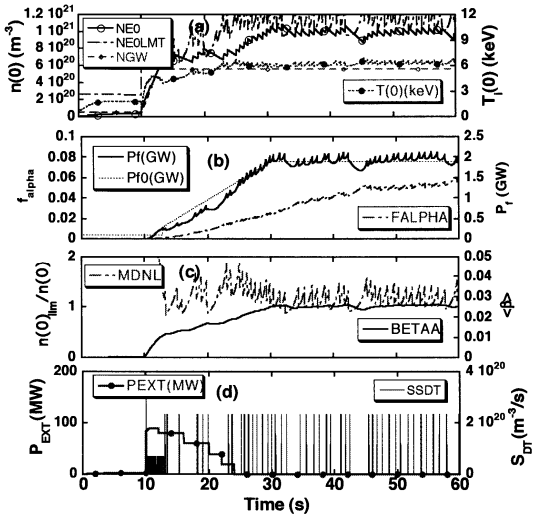

FIG. 5. Temporal evolution of the plasma parameters with the pellet size is 16 mm. (a) -(d) are the same as in Fig. 3.

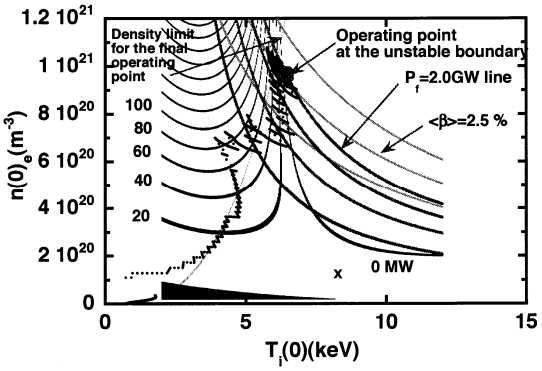

FIG. 6. The operation path to the unstable ignition point on POPCON corresponding to Fig. 5.

ignition is still maintained. The variation of the fusion power is also increased. In POPCON, the operation point oscillates almost in parallel with the constant beta line. This means that control cannot be done by the beta value. For the larger pellet size of 17 mm, the density

variation is slightly larger than 16 mm case, but ignition is terminated at t=50 s. At the termination phase, the density and the temperature are both decreased at the same time, and their variations are in phase.

For a large He ash confinement time ratio of τ_α^*/τ_E =8, fuel particle confinement time ratio of τ_p^*/τ_E=3, and γ_{ISS}=1.55 with the 14 mm pellet, ignition is also possible as shown in Fig. 7.

When the fuel particle confinement time ratio is even longer as τ_p^*/τ_E=8, ignition control can be done because the effective fuel particle confinement is shorter due to D-T fusion reactions.

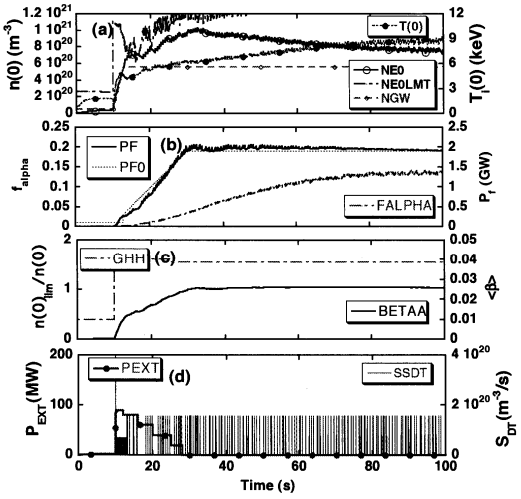

FIG. 7. Temporal evolution of the plasma parameters with pellet injection with 14 mm pellet size and τ_α^*/τ_E =8. (a)-(d) are the same as in Fig. 3 except for (c) the confinement factor and the beta value.

4. Comparisons of the operating parameters with the stable operation

Operating parameters in the stable and unstable ignition regime are compared for the same parabolic density and temperature profiles and the same fusion power in Table 1. Note these values are obtained by continuous fueling. The plasma conduction loss P_L is reduced in the unstable high-density regime due to longer confinement time, and then the divertor heat flux is reduced almost by one half. To compensate the power balance, the bremsstrahlung loss P_B is increased. The beta value is larger in the high-density unstable regime because the plasma energy is larger for the same fusion power due to lower reactivity in the low temperature regime.

For the more peaked SDC profile, the beta value is reduced in comparison with the parabolic case. As the confinement time is also increased, the plasma conduction is further reduced, leading to smaller divertor heat flux of 5.4 MW/m^2 for the 10 cm width divertor plate.

However, SDC plasma tends to show the relatively lower confinement factor in LHD experiments. Therefore, the relations between the confinement enhancement factor γ_{ISS}, the helium ash confinement time ratio τ_α^*/τ_E, and the operating temperature T(0) in ignition are described in Table 2. If the confinement enhancement factor is small as 1.3, for example, the helium ash confinement time ratio should be lower than 4 to have a lower temperature around 7.22 keV for good pellet penetration. For a larger confinement factor of 1.6, the helium ash confinement time ratio should be lower than 5 to have a lower temperature around 7.14 keV for good pellet penetration. To lower the operating temperature for good pellet penetration, the helium ash confinement time ratio should be as small as possible.

TABLE 1. COMPARISON OF THE PLASMA PARAMETERS AT THE STABLE AND UNSTABLE OPERATING POINT

		Steady state value		
		Stable operating point	Unstable operating point	
		Parabolic profile	Parabolic profile	SDC profile
Major radius	R (m)	14.0		
Effective minor radius	$\bar{a}$ (m)	1.73		
Polarity/Field period	ℓ /m	2/10		
Coil pitch parameter	γ	1.15		
Magnetic filed	B_o (T)	6.0		
Maximum magnetic field	B_{omax} (T)	13.3		
Coil magnetic energy	W_c(GJ)	120		
Blanket thickness	ΔB(m)	1.2		
Rotational transform	$\iota_{2/3}$	0.92		
Maximum external heating power	P_{EXT} (MW)	100		
Confinement factor over ISS95 scaling	γ_{ISS95}	1.92		1.6
Confinement time	τ_E (s)	1.9	3.9	4.7
Helium ash fraction	f_α	0.034	0.034	0.058
Oxygen impurity fraction	f_o	0.0075		
Effective ion charge	Z_{eff}	1.48		
He ash confinement time ratio	τ_α^*/τ_E	3		
Fuel particle confinement time ratio	τ_p^*/τ_E	3		
Fusion alpha heating efficiency	η_α	0.9		
Operation density	$n_e(0)$ (10^{20} m^{-3})	2.8	6.0	9.6
Density limit factor over Sudo scaling	γ_{SUDO}	1.5	4.5	5.5
Density limit margin in the steady state	$[n(0)_{limit}/n(0)]$	1.27	1.36	1.59
Ion temperature	$T_i(0)$ (keV)	15.3	8.5	6.4
Ion to electron temperature ratio	T_i/T_e	1.0		
Density profile	α_n	1.0		Box type
Temperature profile	α_T	1.0		0.25
Beta value	$<\beta>$(%)	3.0	3.6	2.5
Plasma energy	W_p(MJ)	547	634	448
Fusion power	P_f (MW)	1900		
Neutron power	P_n (MW)	1520		
Alpha heating power	P_α (MW)	380x0.9		
Bremsstrahlung power	P_B (MW)	57	181	248
Synchrotron radiation power	P_S (MW)	3.4	0.97	0
Plasma conduction loss	P_L (MW)	282	160	96
Electric power output (thermal efficiency)	P_e (MW)	627(33%)		
Neutron wall loading	Γ_n (MW/m^2)	1.5		
Heat flux to first wall	Γ_h (MW/m^2)	0.06	0.18	0.25
Heat flux to divertor for 0.1m wet width	Γ_{div} (MW/m^2)	16	9.1	5.4

5. He ash measurements in normal discharges of LHD

The helium ash confinement time was measured in the normal discharge with the local island divertor (LID) operation with pumping effect for the magnetic axis of R=3.75m and B=2.64T. Even in the normal discharge this type of measurements have not been tried yet in LHD. Therefore, He gas puffing technique and charge exchange recombination

TABLE 2. THE CONFINEMENT ENHANCEMENT FACTOR, HELIUM ASH CONFINEMET TIME RATIO AND OPERATING TEMPERATURE IN IGNITION.

γ_{ISS}	τ_α^*/τ_E	n(0)	T(0)	Z_{eff}	f_α	P_{div}	$<\beta>$
1.2	3.0	6.77×10^{20} m^{-3}	7.77 keV	1.48	3.28	12.1 MW/m^2	2.18
	3.5	6.43	8.12	1.49	3.83	12.6	2.16
1.3	3.0	8.19	6.89	1.49	3.79	9.29	2.33
	4.0	7.84	7.22	1.52	5.01	9.75	2.32
	5.0	7.45	7.62	1.54	6.22	10.3	2.32
	6.0	6.98	8.15	1.56	7.40	11.1	2.30
	6.5	6.67	8.51	1.57	7.99	11.5	2.29
1.4	3.0	8.89	6.59	1.50	4.40	7.63	2.41
	4.0	8.57	6.90	1.53	5.80	8.01	2.42
	5.0	8.23	7.24	1.56	7.17	8.44	2.43
	6.0	7.86	7.65	1.59	8.49	8.96	2.42
	7.0	7.44	8.14	1.61	9.78	9.61	2.42
	7.5	7.19	8.44	1.62	10.41	10.0	2.42
1.5	3.0	9.33	6.46	1.52	5.09	6.45	2.48
	4.0	9.01	6.78	1.55	6.69	6.79	2.48
	5.0	8.66	7.13	1.58	8.24	7.19	2.49
	6.0	8.30	7.53	1.61	9.73	7.67	2.50
	7.0	7.91	8.01	1.64	11.1	8.23	2.51
	7.5	7.70	8.27	1.65	11.8	8.56	2.52
1.6	3.0	9.62	6.41	1.53	5.84	5.55	2.52
	4.0	9.27	6.75	1.57	7.65	5.89	2.53
	5.0	8.91	7.14	1.60	9.39	6.28	2.55
	6.0	8.54	7.57	1.64	11.04	6.74	2.57
	7.0	8.15	8.07	1.67	12.59	7.29	2.59
	7.5	7.94	8.35	1.68	13.32	7.60	2.63

spectroscopy (CXS) with NBI modulation are used in the range of $\bar{n}$ ~0.7×10^{19}m^{-3} and $\bar{n}$ ~1.5×10^{19} m^{-3}.

In Fig.8 is shown the He-II line after subtracting the signal during no NBI phase with $\bar{n}$ ~0.7×10^{19}m^{-3}(#73556). Since we observe the small He-II line signal by CXS without He gas puffing, the source term from the wall is taken into account (#73558). Basically these two shots provide the source term and He ion confinement time. He ion density is initially estimated by the density increment of $\Delta n_\alpha=\Delta n_e/2$ based on the charge neutrality condition, and the initial source term was determined. After initial He ion density rise-up, He ion density decays which was fitted by the solution of the He particle balance equation with initial guessed He source term and He ion confinement time. Using the shot without He gas puffing (#73558), the relation between He source term and He ion confinement time is obtained. To obtain these two final parameters, calculations were iterated. It provides the He ion confinement time τ_α^*=~340 to ~390 ms during the decay phase, and the energy confinement time is τ_E~60 ms during decay phase, yielding τ_α^*/τ_E =~5.7 to 6.5.

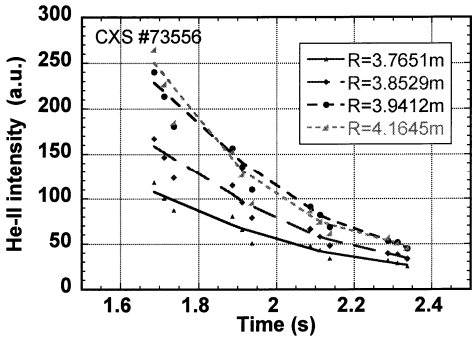

Fig 8. The decay waveform of the He-II line observed by CXS with 40 keV NBI modulation method for $\bar{n}$ *~*0.7×10^{19}*m*$^{-3}$.

In the higher density regime of 1.5×10^{19}m^{-3}, the frame just placed at the front of the CXS detector was adjusted and its opening time was narrowed to remove the detector saturation by the strong light emitted from the plasma edge during He gas puffing. The similar decay signal of He-II line is shown in Fig. 9 after subtracting the signal during no NBI phase

(#81965). As the He ion density without He gas puffing (#81962) is observed larger than that in the lower density case (#73558), iterated calculations provide the slightly shorter He ion confinement time τ_α*=~280 to ~450 ms during the decay phase. For the energy confinement time of τ_E~50 ms during decay phase, it yields τ_α*/τ_E =~5.6 to 9.0. The plume effect (the He^+ ions created by NBI emits the same He-II line by the electron impact excitation along the magnetic field line) would be taken into account in the future analysis.

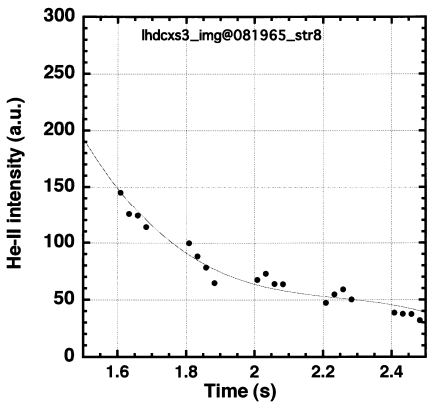

Fig 9. The decay waveform of the He-II line at R=4.05m for $\overline{n}$ =1.5x10^{19}m^{-3}.

6. Comparison between FFHR parameters and LHD experimental data,

In Fig.10 the experimentally achieved values and required plasma parameters for the high-density operation are compared. The temperature, density, beta, confinement factor etc are close to the presently but not simultaneously achieved values. The divertor heat flux is also in the present technology range. Although allowable maximum helium ash confinement time ratio of τ_α*/τ_E~8.0 in this proposed high-density operation is larger than the experimental value (Fig. 10), further reduction of the experimental value is desired for lower temperature operation for easing pellet injection.

Thus we reach conclusion that the LHD type helical reactor with the low temperature and high-density operation is quite promising for a D-T fusion reactor.

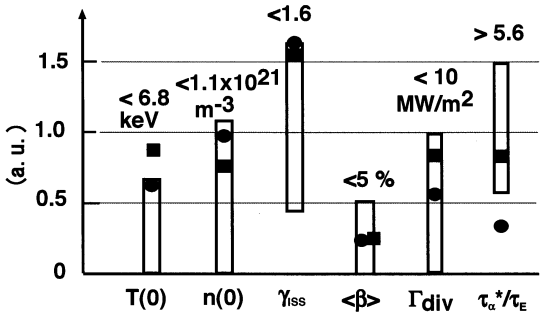

Fig. 10. Comparison of experimentally achieved but independently observed values in LHD (open rectangular) and parameters in the high-density helical reactor (Solid circle corresponds to Fig. 3, and solid square to Fig. 7 with τ_α/τ_E~8.0).*

References

[1] OHYABU, N., et al., Phy. Rev. Lett., 97 (2006) 055002-1.
[2] SAKAMOTO, R., et al., in this IAEA conference, (2008) EX/8-1Ra.
[3] McCORMIC, K., et al., Phy. Rev. Lett., 89 (2002) 015001-1.
[4] MITARAI, O., SAGARA, A., et al., Plasma and Fusion Research, Rapid Communication, Vol.2 (2007) 021-1-3.
[5] MAKI, K., Fusion Technology, **10** (1986) 70.
[6] MANDREKAS, J. and STACY Jr., W. M., Fusion Technology, **19** (1991) 57.
[7] BEBHAN, E. and VIETH, U., Nucl. Fusion, **37** (1996) 251.
[8] HUI, W., et al., Fusion Technology, **25** (1994) 318.
[9] SCHUSTER, E., et al., Fusion Science and Technology, **43** (2003) 18.
[10] VITELA, J. E. and MARTINELL, J. J., Plasma Physics & Controlled Fusion, **40** (1998) 295.
[11] MITARAI, O., SAGARA, A., et al., Nucl. Fusion, 47 (2007) 1411.
[12] SOUERS, P.C., "Hydrogen Properties for Fusion Energy", University of California Press (1986) p80.
[13] MITARAI, O., et al., Fusion Engineering and Design, **70** (2004) 247.